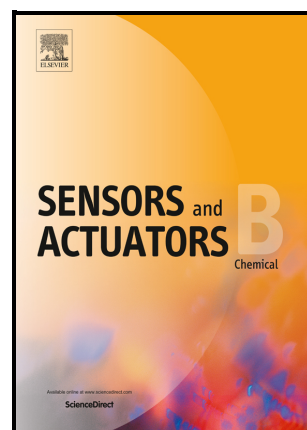


Elsevier required licence: © <2021>. This manuscript version is made available under the CC-BY-NC-ND 4.0 license <http://creativecommons.org/licenses/by-nc-nd/4.0/>
The definitive publisher version is available online at <https://doi.org/10.1016/j.snb.2021.130994>

Simultaneous Multi-Analyte Sensing Using a 2D Quad-Beam Diffraction Smartphone Imaging Spectrometer

Protik Chandra Biswas, Saptami Rani, Md Arafat Hossain, Md Rafiqul Islam, John Canning



PII: S0925-4005(21)01562-8

DOI: <https://doi.org/10.1016/j.snb.2021.130994>

Reference: SNB130994

To appear in: *Sensors and Actuators: B. Chemical*

Received date: 25 July 2021

Revised date: 26 September 2021

Accepted date: 23 October 2021

Please cite this article as: Protik Chandra Biswas, Saptami Rani, Md Arafat Hossain, Md Rafiqul Islam and John Canning, Simultaneous Multi-Analyte Sensing Using a 2D Quad-Beam Diffraction Smartphone Imaging Spectrometer, *Sensors and Actuators: B. Chemical*, (2021) doi:<https://doi.org/10.1016/j.snb.2021.130994>

This is a PDF file of an article that has undergone enhancements after acceptance, such as the addition of a cover page and metadata, and formatting for readability, but it is not yet the definitive version of record. This version will undergo additional copyediting, typesetting and review before it is published in its final form, but we are providing this version to give early visibility of the article. Please note that, during the production process, errors may be discovered which could affect the content, and all legal disclaimers that apply to the journal pertain.

© 2021 Published by Elsevier.

Simultaneous Multi-Analyte Sensing Using a 2D Quad-Beam Diffraction Smartphone Imaging Spectrometer

Protik Chandra Biswas^{1,*}, Saptami Rani¹, Md Arafat Hossain¹, Md Rafiqul Islam¹, and John Canning²

¹Department of Electrical and Electronic Engineering, Khulna University of Engineering & Technology, Khulna 9203, Bangladesh

²interdisciplinary Photonics Laboratories, School of Electrical and Data Engineering, The University of Technology Sydney, NSW 2007, Australia

*Corresponding author: protik@eee.kuet.ac.bd

Abstract:

A multichannel smartphone spectrometer exploiting multiple identical diffraction orders of a customized 2D diffractive element is reported. The instrument utilizes diffraction grating holographic imaging to converge and capture the multiple diffraction orders simultaneously within the limited field-of-view of the smartphone's camera detector. This eliminates the requirement of convergence optics as used in conventional spectrometer systems. Each diffraction order can be utilized as a single optical channel for spectroscopic analysis. As proof of concept, a customized 2D grating composed of two identical thin-film 1D gratings orthogonally stacked together is utilized to diffract the light rays emanating from a broadband visible source and produce four identical 1st orders dispersive diffraction in two orthogonal axes. The smartphone camera captures the diffraction orders within its solid angle – a quad-channel spectrometer exploiting the 2D properties of a CMOS detector is demonstrated. Mindful of losses, further increases in channel numbers is possible by simply increasing the number of gratings (N) within the stack spatially separated by an angle $\theta_N = 180^\circ/N$ between successive grating axes. The instrument offers an ultra-low-cost, lightweight, high throughput, rugged and small form factor multichannel spectrometer ideal for field use as well as a laboratory benchtop alternative. To evaluate the performance of the instrument, three chemically and biologically significant parameters are measured simultaneously: - (a) iron concentration [Fe], (b) chlorine concentration [Cl], and (c) pH of the drinking water.

Keywords: 2D diffraction grating imaging, DPD-Würster compound, $\text{Fe}(\text{phen})_3^{2+}$ complex, multiple analytes, multichannel spectrometer, smartphone sensing.

1. Introduction

Accurate diagnostics of public health systems often require multiple measurements largely using multiple sensors and devices working collectively to extract the detailed physiological and chemical information from different environmental sources and their associated dynamics for a better understanding of the eco-system [1]. Traditional approaches of detecting the multiple information require either recurrent and repeated measurements one after the other with the same instrument or a large number of single sensor devices. They can, through extended time and analysis, incur additional costs, complexity involving slow processing times, parameters that make measurements cumbersome for largescale field deployment in environmental, agricultural, natural disaster monitoring, mapping, and tracking. Smartphones, mostly used in-pocket electronic device, can be an appropriate instrument platform for multi-sensing within a smart-grid sensor network [2, 3]. The advantages are not only their rich choice of sensors and low-cost wireless platform but also their accessibility as an edge internet-of-things (IoT) computational tool aided by networking capabilities [4].

The diagnosis using a smartphone was initially driven by simple colorimetric and microscopic imaging where the complementary metal-oxide-semiconductor (CMOS) camera of a smartphone is used for the optical readout, exploiting the red, green, and blue (RGB) color channels [5-7]. The recent integration of low-cost dispersive elements is harnessing powerful spectroscopic measurements which allows a user to extract multiple information from a single measurement

spectrally over a detectable bandwidth. Further, specially designed optics such as 3D-printable lenses, prisms, slits, diffusers, sample holders and fiber-optics guides have some added advantages in terms of miniaturization, integration, cost, and flexibility of the instrument [8-12]. Presently, most of the smartphone spectrometers reported so far are designed for single parameter detection of a sample utilizing a single channel [13-16]. This means additional measurements are done sequentially. Multifunctional instruments having dual-mode single-channel measurement provision are also reported [13, 49]; a dual-functional smartphone-based sensor was reported for colorimetric and chemiluminescent detection [49]. However, in many practical applications such as in forensic analysis and environmental pollution monitoring, accurate diagnosis requires the detection of multiple parameters simultaneously in an identical setup and environment. This is critical for improving accuracy, referencing, and reliability as well as ensuring comparability.

There are a number of smartphone spectrometers reported to achieve multichannel detection by utilizing beam splitting nano-optics [17, 18], and specially designed dispersive elements [19-21]. A second source and detector are also added in some devices including for benchtop spectrophotometers [22]. However, many of these have major challenges that affect overall instrument performance including the need for specially design optics, alignment between channels without interference, accounting for intensity variation among the channels, poor light collection, and stray light incorporation. We have recently addressed some of these challenges by demonstrating a novel concept of smartphone-based multichannel spectrometer that exploits the multiple diffraction orders of an ordinary one-dimensional (1D) diffraction grating [23, 24]. As a proof-of-concept, a dual-channel absorption spectrometer was demonstrated utilizing two diffraction orders: the +1 and - 1 orders which have the highest intensity and are identical in nature. The second channel successfully produced a spectrum of the background (reference) signal used for absorption measurement of the sample using the Beer-Lambert law. Despite this successful approach, two key challenges remain in further increasing the number of channels: (1) size and light intensity variation between the successive diffraction orders and (2) limited field-of-view (FOV) of the smartphone camera for the increased number of channels where extension in the 1D plane is necessary. The first issue is mainly associated with the properties of diffraction grating where the losses increase dramatically for higher-order modes.

Here, a novel concept of two-dimensional (2D) diffraction grating imaging based spectral analysis is proposed to address the above challenges of conventional 1D grating based spectrometers. The first challenge is resolved by incorporating a 2D diffraction grating array that can serve as both beam splitter and dispersive element; multiple identical diffraction orders can be generated not in 1D but in 2D, an outcome from the grating lattice geometry [25-29]. 2D diffraction gratings with uniform grating pitch have already received great attention due to their ability to separate incident light into its constituent wavelength components in two orthogonal axes [30-32]. For example, 2D diffraction grating with rectangular lattice generates four identical diffraction orders in the orthogonal axes [25, 31]. The second challenge associated with the convergence of multiple orders onto the limited FOV of the smartphone camera can be minimized by utilizing the technique of diffraction grating imaging. In this technique, the diffracted rays are periodically imaged in the form of a 2D array of virtual image called a parallax image array. The spatial separation between parallax images can be tuned not only using the grating parameters but also the position of the point source from the grating surface [33-36]. The technique overall offers great flexibility over the traditional approach of 3D imaging including camera array, lens array, or moving camera, and used in a range of applications such as 3D data processing, 3D profiling, 3D display, and so on [35, 37-39]. In particular, it eliminates the need for additional convergence optics such as lens, mirrors, or especially designed gratings (for example, concave blazed gratings and Fresnel gratings) as used in the traditional benchtop and smartphone spectrometers. This will further reduce the cost and increase the throughput with small form factor, and the overall robustness of spectrometer devices for many field-portable operations, especially in a resource-limited setting.

In this work, a multichannel smartphone spectrometer is designed by utilizing a 2D grating having multiple identical diffraction orders that form a holographic image onto the smartphone camera. As a proof of the concept, a quad-channel spectrometer is demonstrated to monitor the absorption profiles of three different parameters simultaneously in three channels that are regarded as chemically significant to assess drinking water quality (iron, chlorine and pH). The fourth channel of this spectrometer is used as the reference channel. A smartphone application (app) allows measurements in fields and reporting results thus allowing an immediate response. Further extension of the instrument to achieve higher number of channels are clearly possible.

2. Instrumentation and Calibration

2.1 Optical layout design

The basic layout of the smartphone multichannel spectrometer utilizing a 2D diffraction grating imaging is shown in Fig. 1. A multimode optical fiber light guide ($\phi_F = 1000 \mu\text{m}$, $L_F = 20 \text{ cm}$) and a light coupling set up having a ball lens ($\phi_{BL} = 10.0 \text{ mm}$; $f_{BL} = 7.3 \text{ mm}$) at the starting end of the fiber are used to collect the light from an optical source. The set-up has the provision of selecting the optical source from the blackbody emission of the sun and the in-built white flash LED of a smartphone. The use of sunlight reduces power consumption enabling longer operation in the field whereas the smartphone flash LED facilitates indoor and weather-independent applications. Despite the intensity variation up to an acceptable level, the solar irradiance is utilized providing flatter emission spectrum over $\lambda = 400 \sim 700 \text{ nm}$ compared to the phosphor-converted flash LED emission. Emitted light from the other end of the optical fiber is used as the point source of visible light. A 2D grating is utilized to diffract the light rays emanating from the point source to produce identical diffraction orders in both orthogonal axes. The 2D grating of rectangular lattice structure is simply tailored by two identical thin-film polymer 1D transmission gratings (holographic, groove density $g_D = 1000 \text{ lines/mm}$; Rainbow Symphony) orthogonally stacked together.

The technique can generate $2N$ identical diffractions for a particular order by stacking N number of identical 1D gratings at an equal angular separation $\theta_N = 180^\circ/N$ between the successive gratings as illustrated in Fig. 2. The number of the observable order, spatial resolution, and intensity profile of the diffraction depends on the surface lattice structure defined by N , g_D , and θ_N . For the specified parameters of the gratings, higher diffraction orders of very weak intensity profile are not detected by the CMOS camera of the smartphone [Fig. 2]. In this work, a 2D grating of rectangular lattice structure is utilized to generate four identical diffraction orders that are used for quad-channel spectroscopic measurements. Each of the identical diffraction orders is used as a single channel to measure a sample placed on its propagation way. The diffracted light rays are captured by the CMOS camera sensor of the smartphone as a wavelength-dependent parallax image (PI) array of the point source. Here, the imaging depth of the virtual parallax images is same as that of the point source. The X -coordinate of the parallax image, $PI(x_{m,\lambda}, y_{m,\lambda}, z_o)$ for the particular diffraction order (m) and wavelength (λ) is determined by Eq. 1 from the location of the point source (x_o, y_o, z_o) and the distance (L) between the grating and the in-built imaging lens of the smartphone ($0, 0, 0$) as shown in Fig. 3. The Y -coordinate $y_{m,\lambda}$ of a parallax image is obtained by simply replacing x_o with y_o in Eq. 1. The imaging point $I(x_{m,\lambda}, y_{m,\lambda}, z_o)$ on the parallax image pick-up plane is given by Eq. 2, where z_I stands for the Z -coordinate of the pick-up plane. Although the ray reaching $I(x_{m,\lambda}, y_{m,\lambda}, z_o)$ in the pick-up plane seems to come from $PI(x_{m,\lambda}, y_{m,\lambda}, z_o)$, only the rays emanating from the point source are real. The virtual rays coming from the parallax image to the optical center of the imaging lens meet the diffraction grating at the point given by a position function $G(x_{m,\lambda}, y_{m,\lambda}, z_o)$, as equated by Eq. 3 [35, 37].

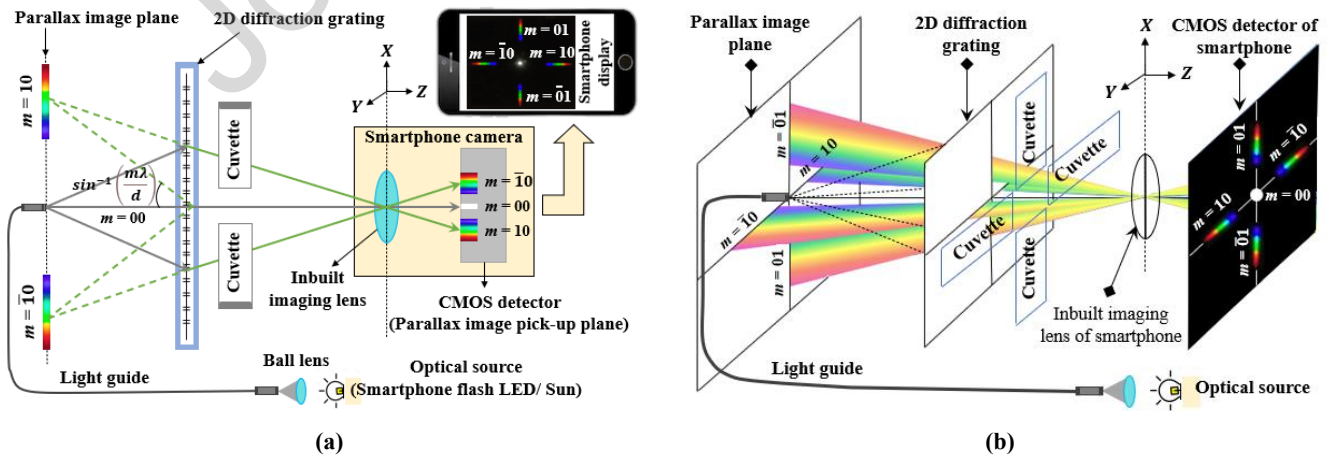


Fig. 1. The optical layout of multichannel smartphone spectrometer: (a) 2D top view; the side view is identical to the top view, and (b) 3D illustration.

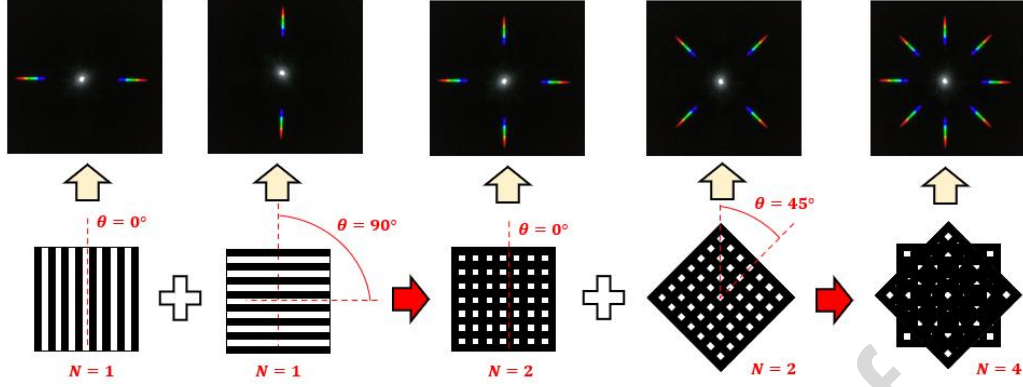


Fig. 2. $2N$ identical multiple diffraction orders generation from 2D grating stacked by N number of identical thin-film 1D diffraction gratings ($g_D = 1000$ lines/mm).

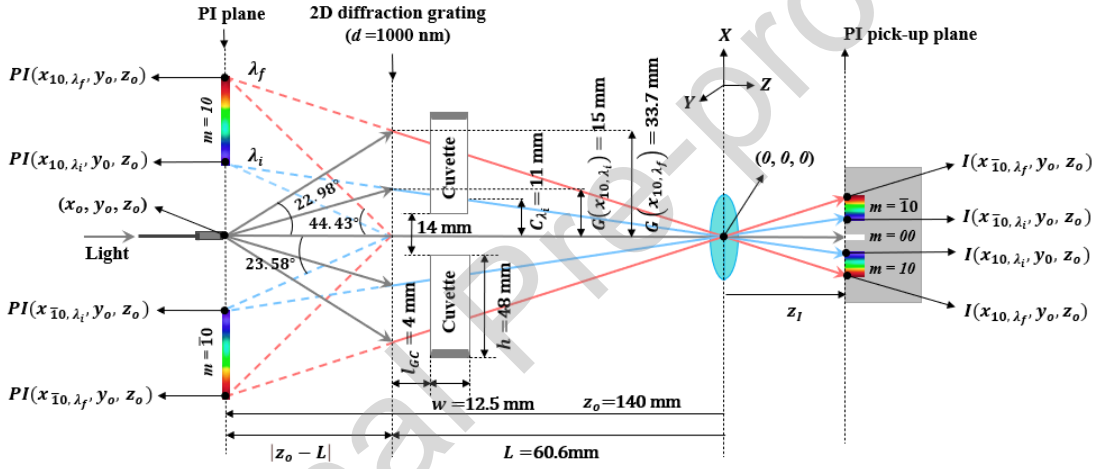


Fig. 3. Illustrate diffraction grating imaging to capture four identical diffraction orders passing through the cuvettes as the parallax images by the CMOS camera detector.

$$x_{m,\lambda} = x_o + |z_o - L| \tan(\sin^{-1}(g_D m \lambda)) \quad (1)$$

$$I(x_{m,\lambda}, y_{m,\lambda}, z_o) = \left(\left(\frac{z_1}{z_o} \right) x_{m,\lambda}, \left(\frac{z_1}{z_o} \right) y_{m,\lambda}, z_1 \right) \quad (2)$$

$$G(x_{m,\lambda}, y_{m,\lambda}, z_o) = \left(\left(\frac{L}{z_o} \right) x_{m,\lambda}, \left(\frac{L}{z_o} \right) y_{m,\lambda}, L \right) \quad (3)$$

Design parameters of the instrument are calculated using Eqs. 1-3 and considering a bandwidth $\Delta\lambda = \lambda_i - \lambda_f = (400 - 700)$ nm, $g_D = 1000$ lines/mm and minimum clearance $C_{\lambda_i} = 11$ mm for the lowest wavelength component λ_i from the optical axis at the outer edge of the cuvette. The clearance is chosen by considering the dimension $(12.5 \times 12.5 \times 48)$ mm of a standard cuvette of 1 cm optical path length and the minimum spacing of placement $x = y = (14 \times 14)$ mm among the four cuvettes corresponds to each optical channel. Utilizing the parameter of C_{λ_i} , $G(x_{m,\lambda_i})$ is calculated by using Eq. 4.

$$G(x_{m,\lambda_i}) = \frac{C_{\lambda_i}}{L - l_{GC} - w} \times L = 15 \text{ mm} \quad (4)$$

where, l_{GC} is the distance of the cuvette from the grating and w is the width of the cuvette. Considering the end of the optical fiber as the reference optical axis (i.e., at $x_o = 0$), X-coordinate of the parallax image for the wavelengths λ_i and λ_f can be determined by Eq. 5 and 6 respectively.

$$x_{m, \lambda_i} = 0.4365 \times |z_o - L| \quad (5)$$

$$x_{m, \lambda_f} = 0.9803 \times |z_o - L| \quad (6)$$

By considering Eq. 3 and Eq. 4,

$$x_{m, \lambda_i} = 15 \times \frac{z_o}{L} \quad (7)$$

By solving Eq. 5 and Eq. 7,

$$L^2 - z_o L + 34.3643 z_o = 0 \quad (8)$$

The condition of real roots of the Eq. 8 are given by,

$$z_o^2 - 4 \times 34.3643 z_o \geq 0 \quad (9)$$

The condition of having diffraction orders within the FOV of the smartphone's CMOS camera considering specified cuvette clearance is $z_o > 137.46$ mm. This determines the distance between smartphone's camera to the source (end of the optical fiber) as 140 mm. Distance between smartphone's camera to the grating, $L = 60.6$ mm is calculated by using Eq. 8. X-coordinate of the converging point at the grating for λ_f is $G(x_{m, \lambda_f}) = 33.7$ mm as calculated by Eq. 3 and depicted in Fig. 3. In order to fit all four channels of the 1st order diffraction within the camera FOV, the minimum dimension of the 2D grating will be 67.4×67.4 mm. In our design, a 2D grating of dimension 80×80 mm is used.

2.2 3D design and fabrication

To assemble all optical components in the appropriate positions and keep them aligned with the smartphone CMOS camera module as designed above, a 3D optomechanical attachment for the multichannel smartphone spectrometer is modeled using computer-aided design (CAD) tools [Fig. 4(a)]. A cuvette holder is also designed to accommodate four standard cuvettes of 1 cm optical path length in the way of each 10, $\bar{1}0$, 01 and $0\bar{1}$ diffraction order. The holder works as a cuvette tray to place the samples in the specified cells and then insert them into the allocated slots. To improve light collection efficiency, a customized optocoupler attachment is modeled to hold the light collection ball lens precisely in position with respect to the optical fiber light guide.

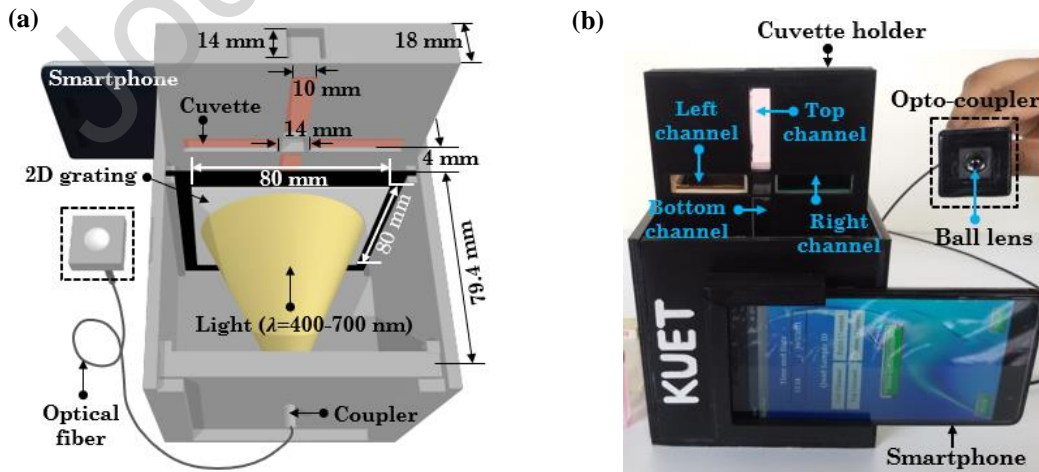


Fig. 4. Quad-channel smartphone spectrometer: (a) the 3D design with integrated optics, and (b) 3D printed device installed on a smartphone; cuvette holder is taken upward to show the cuvettes at the specified channels.

Low-cost polylactic acid (PLA) black filament is used to fabricate the optomechanical and optocoupler attachments and the cuvette tray utilizing the fused deposition modeling (FDM) based 3D printing technology. Finally, the 3D-printed spectrometer attachment is assembled and installed on the smartphone (Xiaomi Redmi Note 4) as shown in Fig. 4(b). The fabricated instrument is robust, inexpensive (< 14 USD), compact, and lightweight (~ 175 gm), designed for field portable measurements.

2.3 Spectrometer App development and calibration

For the proper functionality of the instrument in a smartphone platform, a customized Android app is developed. The workflow of the app to perform real-time measurements in multiple channels is illustrated in Fig. 5. At first, in the registration screen of the app, sample ID with corresponding refractive index is inserted for each of the quad channels. The app then adjusts the rear facing camera of smartphone according to the predefined settings at a fixed focus and -1.00 EV exposure compensation to produce a 2D image of 2976×2976 matrix of pixels that show the multi-color band of the diffracted light. In the image processing section, the spectrum of each channel corresponding to the defined diffraction orders is cropped from the 2D image, and a specific region of interest (ROI) is selected on each spectrum. A calibration algorithm is applied to determine the intensity (I) of each RGB pixel along the diffraction direction and plot them as I vs λ . The algorithm considers both nonlinear wavelength increment along the diffraction direction and additional drift due to refractive index variation of the sample and the holders as discussed in our previous work [24]. A spectral resolution of $\delta\lambda = 1$ nm is achieved by considering the specification and position of the grating with respect to the detector, utilized orders of diffraction, and the specification of CMOS detector with imaging lens according to our previous study [24].

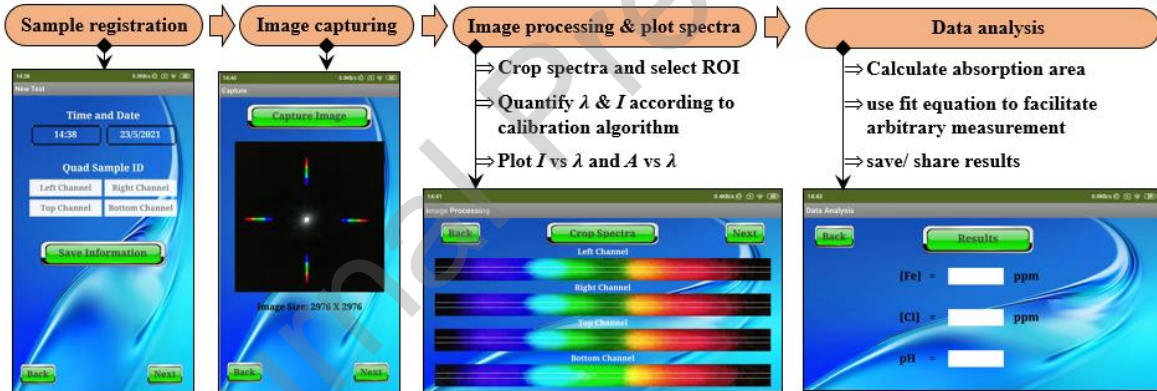


Fig. 5. Workflow of the customized quad-channel smartphone spectrometer app; inset shows the screenshots of the app.

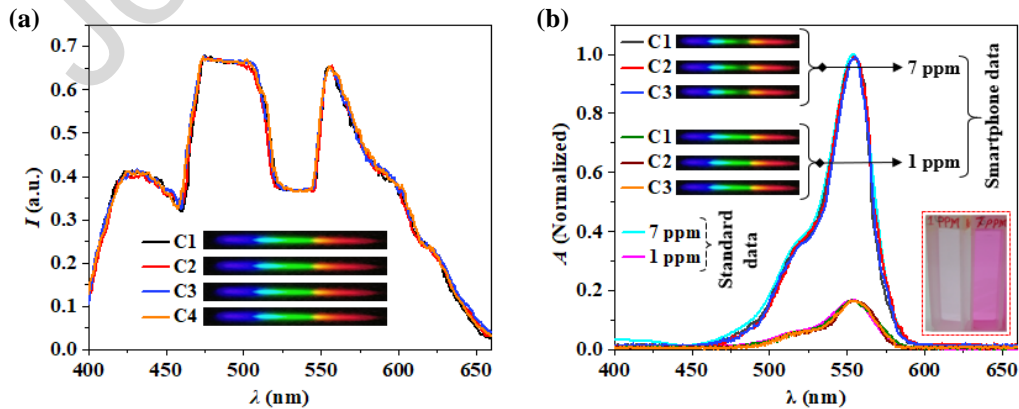


Fig. 6. (a) Solar emission spectral (on 09 April 2021 at 22.90° N, 89.50° E) response recorded by the four channels of the smartphone spectrometer; (b) absorbance spectra of Rhodamine B measured on smartphone and commercial benchtop spectrometers.

The performance of the app to reproduce a result in different channels was evaluated by measuring the visible emission spectrum of the sun simultaneously in four channels. The app satisfactorily measures the emission spectrum identical in all of the four channels [Fig. 6(a)]. Furthermore, the absorption spectra of a laser dye, Rhodamine B (RhB) at two different concentrations [RhB] = (1 and 7) ppm are also measured where three samples were placed in three different channels and the reference was measured in the fourth channel. The results are compared against a commercial benchtop (UV-1800, Shimadzu) spectrometer measurements to validate the absorption response of the channels [Fig. 6(b)]. The app also allows measurement of an unknown sample from a known correlation with their spectral response and sharing the results with others.

3. Performance Evaluation of the Instrument

To evaluate the performance of the smartphone multi-channel spectrometer, it was used to take three simultaneous measurements of water: the concentration of metal ions such as iron [Fe], disinfecting halogen chlorine [Cl], and acidity or alkalinity (pH). These are particularly important and when combined they provide an assessment of the physical, chemical, and biological properties of drinking water. The instrument has been applied to measure them via absorption spectroscopy where three channels were used for samples and the fourth channel was used for background (reference) measurements. The results of the measurement in the individual channel for a specific parameter are discussed below.

3.1 [Fe] measurements

Iron is a biological micronutrient essential for most living organisms, acting as a cofactor for enzymes to assist in fundamental metabolic processes. A significant portion of body iron requirement is fulfilled by drinking water where iron can exist in both ferric (Fe^{3+}) and ferrous (Fe^{2+}) forms. Fe^{3+} exists in surface water and comes mostly from industrial waste whilst Fe^{2+} is naturally present in underground water. Although high concentration ($[\text{Fe}] < 3.0$ ppm) of iron is not always toxic, sometimes it works as a helpful agent identifying the presence of other hazardous metals ions in drinking water. However, $[\text{Fe}] > 0.3$ ppm can cause iron bacteria growth resulting pipe clogging and can introduce a bad odor and metallic taste of water [40]. Therefore, a regular monitoring of [Fe] in drinking water is important. To determine the [Fe] in water, 5 standard samples were prepared by dissolving anhydrous FeCl_3 in distilled water at different concentrations ($[\text{Fe}] \sim 0.5$ -5.0 ppm). Hydrolysis of FeCl_3 dissociates as Fe^{3+} and Cl^- ions and forms a yellowish solution. The commercially available 1,10-phenanthroline ($\text{C}_{12}\text{H}_8\text{N}_2$) is added into the solution as an iron probe which forms a strong reddish-orange colored $\text{Fe}(\text{phen})_3^{2+}$ complex, also known as ferroin, through chemical bonding with Fe^{2+} [41, 42]. Fe^{3+} is first reduced to Fe^{2+} by using a reducing agent – sodium sulphite (Na_2SO_3) because $\text{C}_{12}\text{H}_8\text{N}_2$ is only sensitive to Fe^{2+} . The intensity of the color complex increases with $[\text{Fe}^{2+}]$. Finally, the total iron concentration within the prepared samples is confirmed by a standard checker disc (HI 38040, Hanna Instrument).

Spectroscopic measurement of the prepared standard iron samples is performed and the corresponding absorbance spectra measured by both benchtop and smartphone spectrometers are plotted in Fig. 7(a). Both of the measurements are in a good agreement within the working range and show a broad visible absorption band with peak at $\lambda_p \sim 510 \pm 2$ nm due to the formation of $\text{Fe}(\text{phen})_3^{2+}$ color complex. An empirical equation relating the absorbance area (K) and [Fe] can be obtained [Fig. 7(b)] and uploaded to the smartphone app for determination of [Fe] of unknown samples within the limit.

3.2 [Cl] measurements

Chlorine comes into the surface and drinking sources mainly from chlorination of the water – the use of bleach chemicals, typically hypochlorous acid (HOCl) for disinfecting bacteria, fungi, viruses, and other harmful pathogens. However, highly chlorinated water ($[\text{Cl}] > 5.0$ ppm) can produce harmful carcinogenic trihalomethanes as a by-product element that causes cell damage. Therefore, a routine monitoring of [Cl] is essential to ensure a safe water ecosystem ($2 \sim 4$ ppm) [40]. To measure chlorine, 5 standard samples of $[\text{Cl}] \sim 0.7$ to 10 ppm were prepared by dissolving calcium hypochlorite ($\text{Ca}(\text{OCl})_2$) in distilled water.

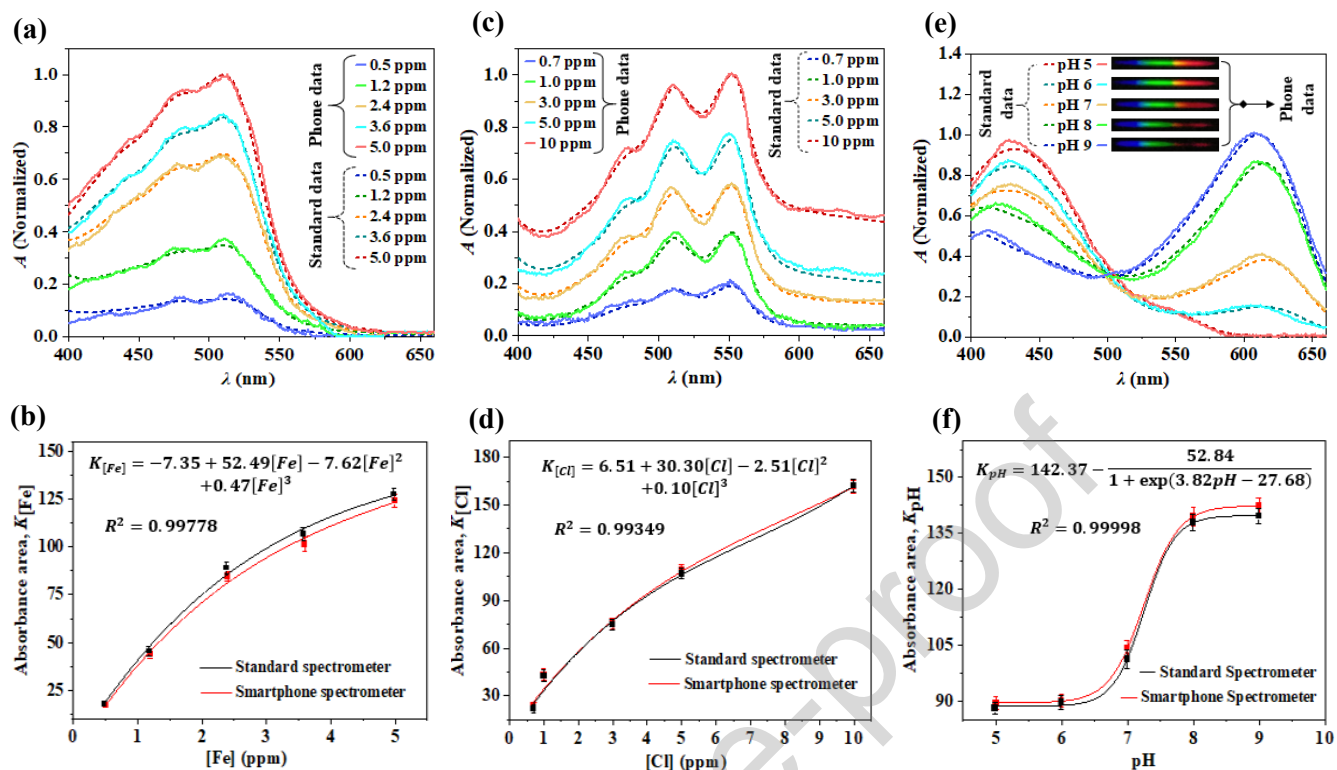


Fig. 7. Absorbance spectra of (a) $\text{Fe}(\text{phen})_3^{2+}$ complex at differently concentrated iron solutions, (c) DPD Würster compound at differently concentrated chlorinated water and (e) different pH samples in presence of universal pH indicator. The polynomial fit plot of (b) absorbance area vs $[\text{Fe}]$, (d) absorbance area vs $[\text{Cl}]$ and (f) Boltzman fit curve of absorbance area correspond to pH value. The error bars illustrate the relative standard deviation over three measurements of the same samples.

The solution dissociates and releases free chlorine as HOCl or OCl^- . As a strong oxidizing agent, free chlorine reacts with various chemical contaminants in water, mostly nitrogenous compounds (e.g. ammonia, nitrites, and amino acids) and leads to the formation of chloramines (monochloramine, dichloramine, and trichloramine) depending on the pH and temperature of the water. Production of chloramines converts free chlorine into combined chlorine and the total $[\text{Cl}]$ is the summation of the two forms. A commercially available low-cost colorimetric probe, DPD (N,N-diethyl-p-phenylenediamine), is used as a chlorine indicator that reacts with free chlorine in the presence of dissolved oxygen and turns the solution into a pinkish color. Potassium iodide (KI) is also added into the solution to react with the combined chlorine. The chloramines oxidize the iodide and release iodine that reacts with DPD to further contribute the pink color by forming the Würster complex [43]. The intensity of the color is directly proportional to the total $[\text{Cl}]$ present in the solution. The final concentration is also confirmed by a checker disk (HI 38020, Hanna instrument).

The absorption spectra of DPD-Würster compound for differently chlorinated water were measured in the second channel of the smartphone spectrometer and also in a benchtop spectrometer [Fig. 7(c)]. The color complex absorbs light within the visible band with the doublet absorption peaks at $\lambda_p \sim 512 \pm 3$ and $\sim 553 \pm 5$ nm. The Würster color complex strongly absorbs the green light ($\lambda_p \sim 553$ nm) and excites the photons to the lowest electronic excited state (D_1). Due to a small energy gap between the D_1 and the D_0 (ground state), at room temperature, the free radical cation of Würster dye transits to the more stable D_0 state within few picoseconds and consequently shifts the absorbance peak at $\lambda_p \sim 512$ nm. This transition between two absorbance maxima is held by the transfer of the unpaired valence electron from the amino groups toward the phenyl group [44]. A calibration equation is obtained by correlating the absorbance area with the $[\text{Cl}]$ as shown in Fig. 7(d).

3.3 pH measurements

Drinking water with a balanced pH level (pH ~ 6.5 to 8.5) is critically important to regulate body metabolic processes and beyond this range, it will be detrimental for health [40]. The knowledge of pH is also important for perfect disinfection of water system that ensures adequate chlorine in residual form within the drinking water to continue disinfecting action [45]. To measure water pH, a total of 5 buffer solutions ranging from pH ~ 5 to 9 are prepared by titration of standard acetate and phosphate buffer using 0.1 M sodium hydroxide (NaOH) at room temperature $T \sim 25$ °C. The pH value of each buffer solution is further confirmed by using a properly calibrated standard pH meter (Ezodo PH5011). Finally, for colorimetric readout of the sample pH, 0.1 ml of universal indicator is added to 10 ml of each buffer solution which gives a distinct color of each sample. The intensity of the colored pH solution is proportional to the concentration of the pH indicator. The measured absorbance spectra of the pH solutions using both standard and smartphone spectrometer are plotted in Fig. 7(e). Due to the protonated and deprotonated form of the pH probe molecules, the absorbance spectra show two distinct absorbance bands with duplet absorbance peaks at $\lambda_p \sim 429$ and 610 nm respectively as the pH of the buffer solutions shift from acidic to basic [46]. pH value and the acid dissociation factor (pKa) of the probe molecules have a great influence on the absorption peak. The solution with pH greater than pKa of universal indicator (~ 8.27) shows λ_p in the red band whereas solution with pH less than pKa absorbs blue light significantly [47]. Moreover, a redshift of $\Delta\lambda = 20$ nm is measured for the blue absorption peak as the pH of the solution is increased from 5 to 9. The relative absorbance area for each sample is plotted and the Boltzman fit function is obtained for the pH values [Fig. 7(f)]. To determine the calibration equation for the three different tests, firstly the absorbance response recorded by the smartphone spectrometer is normalized with respect to each channel and then the calculated absorbance area is utilized as the independent explanatory variables of regression analysis corresponds to the study variables [Fe], [Cl] and pH.

For these three different tests, limit of detection (LoD), range, sensitivity and accuracy of the measurement are illustrated in Table-1. The LoD is estimated based on a signal-to-noise ratio of 3:1 according to the guidelines of International Council for Harmonisation (ICH) [48]. Sensitivity is determined through the regression analysis method. The spectral response and so the test performance can be affected by the variation of the light intensity as well as the concentration of the reagent used in the sample as illustrated in Fig. 8(a) and (c) respectively. The impact of light intensity variation can be significant in the case of solar illumination which changes over time and location. Figure 8(a) depicts that for a specific band of RGB intensity ($I_{av} = 0.2 \sim 0.9$), performance parameters are not altered with the intensity variation of the light source whereas beyond this band test performance deteriorates significantly. This is due to the non-monotonical changes of RGB values of samples and references at the edges and also the poor signal-to-noise ratio at low light intensity. The average RGB intensity (I_{av}) is calculated considering the normalized RGB values of the i^{th} pixel for the defined ROI of N pixels on the spectrum of fourth channel according to Eq. 10.

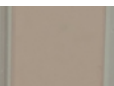

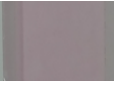



$$I_{av} = \frac{\sum_{i=0}^N \left(\frac{R_i}{255} + \frac{G_i}{255} + \frac{B_i}{255} \right) / 3}{N} \quad (10)$$

I_{av} not only depends on the ambient intensity (A_I) but also the collection angle of the opto-coupler, sensitivity of the CMOS detector and the losses occurred in optics used in the spectrometer. At $I_{av} \sim 1.0$, the smartphone CMOS detector is saturated and incorrect absorbance response is recorded. Similarly, inappropriate spectral response is measured for the value of $I_{av} < 0.2$ [Fig. 8(a)]. For both of these cases LoD, sensitivity and range of the test are found different from the values as specified in Table 1 and are not suggested for use of the instrument as the measurement can be unstable. To ensure stable and accurate measurement, the customized app incorporates a correction algorithm to calculate I_{av} before taking a measurement and to suggest the user whether the light intensity is sufficient (I_{av} in between 0.2 ~ 0.9) or not. In contrast to solar emission, the in-built flash LED as an optical source offers superior stability ($I_{av} \sim 0.76$) ensured by the integrated driver circuit of the smartphone. This is also powered by the in-built battery of smartphone. Overall, the performance obtained using the flash LED are in good agreement with the solar emission-based measurement because of the implementation of source dependent normalization at the time of absorbance measurements [Fig. 8(a)].

In addition to light intensity, the sensitivity of the CMOS detector and the concentration of indicator have significant impact on determining the test performance parameters. As for example, influence of the different amount of universal

indicator for the quantification of pH is illustrated in Fig. 8 (b) and (c). For a water sample of certain pH, the absorbance increases significantly after increasing the concentration of the universal indicator from 0.01 % to 0.04% (v/v). This results about four-fold improvement in the sensitivity of pH measurement as determined from the pH titration curves in Fig. 8(c). The increase of the dye concentration allows the protonation and deprotonation reaction occur at a higher rate with the available indicator molecules in the sample. At the dye concentration beyond this limit, both the detection range and LoD are found degraded.

Table 1. Validation characteristics for the measurement of [Fe], [Cl] and pH of drinking water

Test Name	LoD	Sensitivity	Range		Accuracy
			Lower	Upper	
[Fe]	0.36 (ppm)	23.32 A*nm/ppm			97.5%
[Cl]	0.44 (ppm)	14.12 A*nm/ppm			96.7%
pH	4.0	15.42 A*nm/pH			98.3%

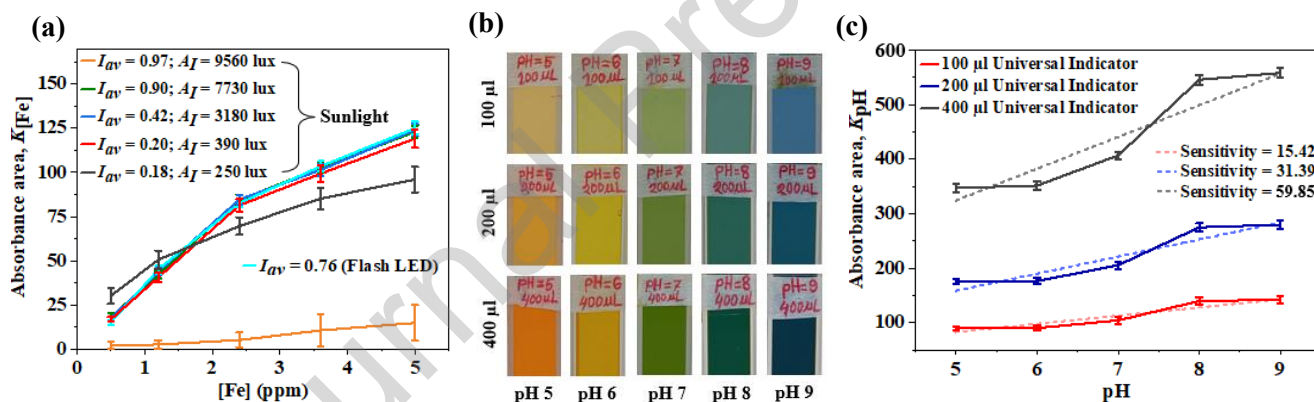


Fig. 8. The influence of light intensity and dye concentrations on the test performance. (a) Influence of light intensity and optical source on [Fe] measurement; (b) 10 ml solution of different pH samples added with different amount of universal indicator; (c) influence of universal indicator on pH measurement. The error bars illustrate the relative standard deviation over three measurements of the same samples.

3.4 Field tests

To evaluate the performance of the smartphone spectrometer for simultaneous measurement of multiple parameters, four water samples were collected from different sources located in Khulna, Bangladesh region. The samples include groundwater (**S1**), surface water (**S2**), purified water (**S3**), and tap water (**S4**). With the above reagents and the designed smartphone quad-channel spectrometer, it is possible to measure three parameters simultaneously via absorption spectroscopy. [Fe], [Cl] and pH of drinking water are measured since these have important health ramifications. For example, the presence of Fe at an extreme level can cause the growth of iron bacteria and many other harmful pathogens. Chlorination is used for disinfection of the pathogens but its performance depends on the pH of the water – it is most effective at slightly acidic pH [45]. Therefore, simultaneous monitoring of these parameters in the sample is important to ensure safe drinking water. To do so, the water sample from source **S1** is taken into three identical vials and placed into the three different channels (C1, C2, and C3). As before, the fourth channel (C4) was used to measure the background signal.

Phenanthroline, DPD, and universal indicator were added to the samples at the predefined concentration as used for [Fe], [Cl], and pH calibration respectively. The prepared solutions, corresponding diffraction images, and recorded absorbance spectra are shown in Fig. 9(a).

After analyzing the measured spectra, the app immediately provides corresponding [Fe], [Cl], and pH values using the calibrated equations described above and then provides a recommendation for the usability of the waters based on the recommended guidelines. For the groundwater sample **S1**, the smartphone measurements provide [Fe] ~1.88 ppm, [Cl] ~ 0 ppm, and pH ~ 7.37. The groundwater normally contains low levels of Cl that falls below the lower detection range ($[Cl] < 0.7$ ppm) of the instrument. Though the significant level of Fe can make this water a bit metallic taste, the [Fe] and pH value remains within the acceptable limit. Following the same procedure, spectroscopic measurements of **S2**, **S3**, and **S4** are also performed as illustrated in Fig. 9(b) – (d). The spectroscopic analysis of the four types of drinking water samples reveals that typically groundwater contains more Fe than the surface and purified water. On the contrary, as surface water (**S2**) is collected for public usage and chlorinated before supplying as drinking water, it contains more Cl (~ 2.78 ppm) for future disinfection against bacteria. Cl is commonly used for water purification and thus purified water contains some Cl content ($[Cl] \sim 1.56$ ppm) but zero or negligibly low Fe due to filtration. Moreover, because of filtering out mineral content, the pH of **S3** becomes slightly acidic (pH~ 6.26) lower than the standard pH range of drinking water. The pH level of tap water (**S4**) collected from a water distribution system is measured as pH ~ 7.72 where both iron ([Fe] ~ 0.52 ppm) and chlorine ([Cl] ~ 0.94 ppm) exist at a low level. The smartphone data of [Fe], [Cl], and pH measurements are in good agreement with the standard meter readings and have an average detection error within the acceptable range ($e_{[Fe]} \sim 2.50\%$, $e_{[Cl]} \sim 3.27\%$ and $e_{pH} \sim 1.68\%$).

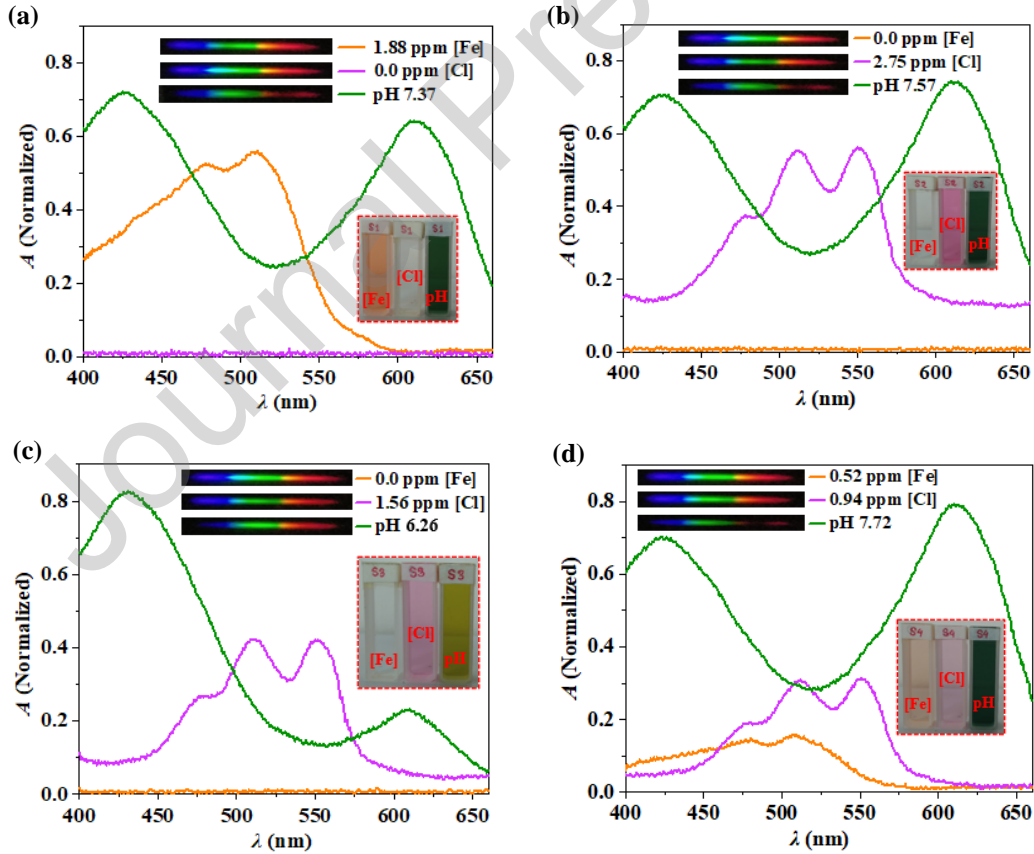


Fig. 9. Multichannel detection of [Fe], [Cl], and pH level in four different types of drinking water samples: (a) **S1**-groundwater, (b) **S2**-surface water, (c) **S3**-purified water, and (d) **S4**-tap water. Inset shows diffraction images correspond to the pictorially represented spectroscopic solutions prepared for measuring [Fe], [Cl], and pH value from each type of water sample.

4. Conclusion

In this work, for the first time, 2D dispersive element and diffraction grating imaging are introduced in smartphone spectrometer to demonstrate multichannel detection. Orthogonally stacking of two ordinary 1D gratings produces four identical diffraction orders, or optical channels, for multichannel measurements and avoids the issues associated with the intensity variation and spectral overlap between adjacent channels of multi-order 1D grating spectrometers. Additionally, diffraction grating imaging converges the diffracted light of broadband source within the limited FOV of smartphone CMOS detector. This overcomes the need for costly and complex light-converging optics as used in many benchtop spectrometers. The 3D-printed smartphone attachment including the customized portable cuvette holder makes the spectroscopic platform rugged and field-worthy and reliable for multiple sample measurements. The performance of the instrument has been validated by measuring three important parameters relevant to safe drinking water: [Fe], [Cl], and pH which together determine the physical, chemical, and biological health of a water system. The real-time detection of all these parameters based on accessible multichannel spectroscopy is essential to develop a highly reliable, real-time water quality monitoring system at the consumer end, offering democratization of technology that empowers people to identify problems of immediate concern to their community. Water safety is paramount in many regions of the world particularly after disasters such as cyclones, flooding, reactor leaks, and more. The instrument can also serve across other sectors including multi-parameter sensing of food quality, soil analysis, and biomedical species. As an edge IoT instrument capable of simultaneous measurements within a small form factor that is swarm compatible, it accelerates diagnostics anywhere in the field, across the industry, or in the laboratory allowing regional and global maps to be compiled [49, 50]. Further, there is room to expand the performance and overall throughput of the instrument by increasing the number of channels with more gratings ($N = 3, 4$, and even more) and customized sample holder with reduced cuvette sizes to fit within the angular space.

Acknowledgments

This work was supported by postgraduate research grants of Khulna University of Engineering & Technology (KUET), Bangladesh.

References

- [1] H. F. Rashvand, and J. M. A. Calero, *Distributed Sensor Systems: Practice and Applications*, Wiley, 2012.
- [2] I. Hussain, and A. K. Bowden, "Smartphone-based optical spectroscopic platforms for biomedical applications: a review," *Biomed. Opt. Express*, vol. 12, no. 4, pp. 1974-1998, Apr. 2021.
- [3] J. Liu, Z. Geng, Z. Fan, J. Liu, and H. Chen, "Point-of-care testing based on smartphone: The current state-of-the-art (2017–2018)," *Biosens. Bioelectron.*, vol. 132, pp. 17-37, May 2019.
- [4] M. Grossi, "A sensor-centric survey on the development of smartphone measurement and sensing systems," *Measurement*, vol. 135, pp. 572-592, Mar. 2019.
- [5] S. Rani, P. C. Biswas, M. A. Hossain, M. R. Islam, and J. Canning, "Polynomial regression of multiple sensing variables for high-performance smartphone colorimeter," *OSA Continuum*, vol. 4, no. 2, pp. 374-384, Jan. 2021.
- [6] C. Song, Y. Yang, X. Tu, Z. Chen, J. Gong, and C. Lin, "A smartphone-based fluorescence microscope with hydraulically driven optofluidic lens for quantification of glucose," *IEEE Sens. J.*, vol. 21, no. 2, pp. 1229-1235, Jan. 2021.
- [7] M. A. Hossain, J. Canning, S. Ast, P. Rutledge, T. L. Yen, and A. Jamalipour, "Lab-in-a-phone: Smartphone-based portable fluorometer for pH measurements of environmental water," *IEEE Sens. J.*, vol. 15, no. 9, pp. 5095-5102, Sep. 2015.
- [8] P. Edwards, C. Zhang, B. Zhang, X. Hong, V. K. Nagarajan, B. Yu, & Z. Liu, "Smartphone based optical spectrometer for diffusive reflectance spectroscopic measurement of hemoglobin," *Scientific Rep.*, vol. 7, Art. no. 12224, Dec. 2017.
- [9] M. A. Hossain, J. Canning, K. Cook, and A. Jamalipour, "Optical fiber smartphone spectrometer," *Opt. Lett.*, vol. 41, no. 10, pp. 2237-2240, May 2016.
- [10] P. Escudero, J. Yeste, C. P. Izarra, R. Villa and M. Alvarez, "Color tunable pressure sensors based on polymer nanostructured membranes for optofluidic applications," *Scientific Rep.*, vol. 9, Art. no. 3259, Mar. 2019.
- [11] C. Zhang, G. Cheng, P. Edwards, M. -D. Zhou, S. Zheng, and Z. Liu, "G-Fresnel smartphone spectrometer," *Lab Chip*, vol. 16, no. 2, pp. 246-250, Nov. 2015.

- [12] A. A. Markvart, L. B. Liokumovich, I. O. Medvedev, and N. A. Ushakov, "Smartphone-Based Interrogation of a Chirped FBG Strain Sensor Inscribed in a Multimode Fiber," *J. Lightwave Technol.*, vol. 39, no. 1, pp. 282-289, Sep. 2020.
- [13] M. A. Hossain, J. Canning, S. Ast, K. Cook, P. J. Rutledge, and A. Jamalipour, "Combined "dual" absorption and fluorescence smartphone spectrometers," *Opt. Lett.*, vol. 40, no. 8, pp. 1737-1740, Apr. 2015.
- [14] D. Jian, B. Wang, H. Huang, X. Meng, C. Liu, L. Xue, F. Liu, S. Wang, "Sunlight based handheld smartphone spectrometer," *Biosens. Bioelectron.*, vol. 143, Art. no. 111632, Oct. 2019.
- [15] L. Kong, Y. Gan, T. Liang, L. Zhong, Y. Pan, D. Kirsanov, A. Legin, H. Wan, and P. Wang, "A novel smartphone-based CD-spectrometer for high sensitive and cost-effective colorimetric detection of ascorbic acid," *Anal. Chimica Acta*, vol. 1093, pp. 150-159, Jan. 2020.
- [16] M. A. Hossain, J. Canning, and Z. Yu, "Fluorescence-Based Determination of Olive Oil Quality Using an Endoscopic Smart Mobile Spectrofluorimeter," *IEEE Sens. J.*, vol. 20, no. 8, pp. 4156-4163, Apr. 2020.
- [17] S. C. Lo, E. H. Lin, K. L. Lee, T. T. Liang, J. C. Liu, P. K. Wei, and W. S. Tsai, "A Concave Blazed-Grating Based Smartphone Spectrometer for Multichannel Sensing," *IEEE Sens. J.*, vol. 19, no. 23, pp. 11134-11141, Dec. 2019.
- [18] R. Bogucki, M. Greggila, P. Mallory, J. Feng, K. Siman, B. Khakipoor, H. King, and A. W. Smith, "A 3D-Printable Dual Beam Spectrophotometer with Multiplatform Smartphone Adaptor," *J. Chem. Educ.*, vol. 96, no. 7, pp. 1527-1531, Jun. 2019.
- [19] L. J. Wang, Y. C. Chang, R. Sun, and L. Li, "A multichannel smartphone optical biosensor for high-throughput point-of-care diagnostics," *Biosens. Bioelectron.*, vol. 87, pp. 686-692, Jan. 2017.
- [20] Y. Wang, M. M. A. Zeinhom, M. Yang, R. Sun, S. Wang, J. N. Smith, C. Timchalk, L. Li, Y. Lin, and D. Du, "A 3D-Printed, Portable, Optical-Sensing Platform for Smartphones Capable of Detecting the Herbicide 2,4-Dichlorophenoxyacetic Acid," *Anal. Chem.*, vol. 89, no. 17, pp. 9339-9346, Jul. 2017.
- [21] L. J. Wang, N. Naude, Y. C. Chang, A. Crivaro, M. Kamoun, P. Wang, and L. Li, "An Ultra-low Cost Smartphone Octochannel Spectrometer for Mobile Health Diagnostics," *J. Biophoton.*, vol. 11, no. 8, Art. no. e201700382, Apr. 2018.
- [22] T. Owen, "Instrumentation," in *Fundamentals of UV-visible Spectroscopy: A Primer*, Agilent Technologies, 2000, pp. 44-46.
- [23] P. C. Biswas, S. Rani, M. A. Hossain, M. R. Islam, and J. Canning, "Multi-channel Smartphone Spectrometer Using Combined Diffraction Orders," *IEEE Sens. Lett.*, vol. 4, no. 9, Art. no. 4500804, Sep. 2020.
- [24] P. C. Biswas, S. Rani, M. A. Hossain, M. R. Islam, and J. Canning, "Recent Developments in Smartphone Spectrometer Sample Analysis," *IEEE J. Sel. Top. Quant. Electron.*, vol. 27, no. 6, Art. no. 5500212, Apr. 2021.
- [25] T. Shui, L. Li, X. Wang, and W. X. Yan, "One- and two-dimensional electromagnetically induced gratings in an Er³⁺ - doped yttrium aluminum garnet crystal," *Scientific Rep.*, vol. 10, Art. No. 4019, Mar. 2020.
- [26] Z. Liu, L. Shi, T. Pu, H. Li, J. Niu, G. Wang, and C. Xie, "Two-dimensional gratings of hexagonal holes for high order diffraction suppression," *Opt. Express*, vol. 25, no. 2, pp. 1339-1349, Jan. 2017.
- [27] P. Qiao, L. Zhu, W. C. Chew, and C. J. C. Hasnain, "Theory and design of two-dimensional high-contrast-grating phased arrays," *Opt. Express*, vol. 23, no. 19, pp. 24508-24524, Sep. 2015.
- [28] G. A. Kriegsmann, "Complete transmission through a two-dimensional diffraction grating," *Siam J. Appl. Math.*, vol. 65, no. 1, pp. 24-42, Sep. 2004.
- [29] D. Ge, J. Shi, A. Rezk, C. Ma, L. Zhang, P. Yang, and S. Zhu, "Two-Dimensional Hole-Array Grating-Coupling-Based Excitation of Bloch Surface Waves for Highly Sensitive Biosensing," *Nanoscale Res. Lett.*, vol. 14, Art. no. 31, Oct. 2019.
- [30] R. Amano, P. Salamon, S. Yokokawa, F. Kobayashi, Y. Sasaki, S. Fujii, A. Buka, F. Araoka, and H. Orihara, "Tunable two-dimensional polarization grating using a self-organized micropixelated liquid crystal structure," *RSC Adv.*, vol. 8, no. 72, pp. 41472-41479, Dec. 2018.
- [31] C. Xie, L. Shi, H. li, Z. Liu, T. Pu, and N. Gao, "Towards High-Order Diffraction Suppression Using Two-Dimensional Quasi-Periodic Gratings," *Springer Series in Optical Sciences*, vol. 222, pp. 31-53, May 2019.
- [32] M. Zakharova, V. Vlnieska, H. Fornasier, M. Börner, T. D. S. Rolo, J. Mohr, and D. Kunka, "Development and Characterization of Two-Dimensional Gratings for Single-Shot X-ray Phase-Contrast Imaging," *Appl. Sci.*, vol. 8, no. 3, Art. no. 468, Mar. 2018.
- [33] J. Y. Jang, J. I. Ser, and E. S. Kim, "Wave-optical analysis of parallax-image generation based on multiple diffraction gratings," *Opt. Lett.*, vol. 38, no. 11, pp. 1835-1837, May 2013.
- [34] M. Trivi, and H. J. Rabal, "Stereoscopic uses of diffraction gratings," *Appl. Opt.*, vol. 27, no. 6, pp. 1007-1009, Mar. 1988.
- [35] J. Y. Jang, and H. Yoo, "Computational reconstruction for three-dimensional imaging via a diffraction grating," *Opt. Express*, vol. 27, no. 20, pp. 27820-27830, Sep. 2019.
- [36] J. I. Ser, J. Y. Jang, S. Cha, and Se. H. Shin, "Applicability of diffraction grating to parallax image array generation in integral imaging," *Appl. Opt.*, vol. 49, no. 13, pp. 2429-2433, Apr. 2010.
- [37] J. Y. Jang, and H. Yoo, "Image Enhancement of Computational Reconstruction in Diffraction Grating Imaging Using Multiple Parallax Image Arrays," *Sensors*, vol. 20, no. 18, Art. no. 5137, Sep. 2020.
- [38] H. Yoo, J. U. Jang, and J. Y. Jang, "Analysis of imaging characteristics of parallax images in double diffraction grating imaging," *Optik*, vol. 207, Art. no. 163826, Apr. 2020.

- [39] J. Huijts, S. Fernandez, D. Gauthier, M. Kholodtsova, A. Maghraoui, K. Medjoubi, A. Somogyi, W. Boutu, and H. Merdji, "Broadband coherent diffractive imaging," *Nat. Photon.*, vol. 14, pp. 618-622, Jul. 2020.
- [40] "Guidelines for Drinking-water Quality" WHO, 2017.
URL <https://www.who.int/publications/i/item/9789241549950>.
- [41] E. Agustina, J. Goak, S. Lee, Y. Seo, J. Y. Park, and N. Lee, "Simple and Precise Quantification of Iron Catalyst Content in Carbon Nanotubes Using UV/Visible Spectroscopy," *ChemistryOpen*, vol. 4, no. 5, pp. 613-619, Jun. 2015.
- [42] B. Oktavia, L. W. Lim, and T. Takeuchi, "Simultaneous Determination of Fe(III) and Fe(II) Ions via Complexation with Salicylic Acid and 1,10-Phenanthroline in Microcolumn Ion Chromatography," *Anal. Sci.*, vol. 24, no. 11, pp. 1487-1492, Nov. 2008.
- [43] Y. Xiong, J. Tan, C. Wang, J. Wu, Q. Wang, J. Chen, S. Fang, and M. Duan, "A miniaturized evanescent-wave free chlorine sensor based on colorimetric determination by integrating on optical fiber surface," *Sens. Actuators B Chem.*, vol. 245, pp. 674-682, Jun. 2017.
- [44] J. Grilj, P. Buchgraber, and E. Vauthey, "Excited-State Dynamics of Wurster's Salts," *J. Phys. Chem. A*, vol. 116, no. 28, pp. 7516-7522, Jun. 2012.
- [45] F. Ge, L. Zhu, and H. Chen, "Effects of pH on the chlorination process of phenols in drinking water," *J. Hazard. Mater.*, vol. 133, no. (1-3), pp. 99-105, May 2006.
- [46] T. D. Meyer, K. Hemelsoet, V. V. Speybroeck, and K. D. Clerck, "Substituent effects on absorption spectra of pH indicators: An experimental and computational study of sulfonphthaleine dyes," *Dye. Pigment.*, vol. 102, pp. 241-250, Mar. 2014.
- [47] L. E. V. Salgado, and C. V. Hernández, "Spectrophotometric Determination of the pKa, Isosbestic Point and Equation of Absorbance vs. pH for a Universal pH Indicator," *Am. J. Anal. Chem.*, vol. 5, no. 17, pp. 1290-1301, Dec. 2014.
- [48] International Conference on Harmonization of Technical Requirements for the Registration of Pharmaceuticals for Human Use, Validation of analytical procedures: Text and Methodology, ICH-Q2(R1), Nov. 2005.
URL <https://database.ich.org/sites/default/files/Q2%28R1%29%20Guideline.pdf>.
- [49] Y. Xing, Q. Zhu, X. Zhou, and P. Qi, "A dual-functional smartphone-based sensor for colorimetric and chemiluminescent detection: A case study for fluoride concentration mapping," *Sens. Actuators B Chemical*, vol. 319, Art. no. 128254, Sep. 2020.
- [50] M. A. Hossain, J. Canning, S. Ast, P. Rutledge, and A. Jamalipour, "Early warning smartphone diagnostics for water security and analysis using real-time pH mapping," *Photon. Sens.*, vol. 5, no. 4, pp. 289-297, Sep. 2015.

Author Biographies

Protik Chandra Biswas received the B.Sc. and M.Sc. degrees in 2015 and 2017, respectively, in electrical and electronic engineering from the Khulna University of Engineering & Technology (KUET), Khulna, Bangladesh, where he is currently working toward the Ph.D. degree. Since 2018, he has been an Assistant Professor with the Department of Electrical and Electronic Engineering, KUET. His research interests include smartphone spectroscopy, smart sensing and instrumentation, and electrical machine drives. He was the recipient of the University Gold Medal.

Saptami Rani received the B.Sc. and M.Sc. degrees in 2016 and 2019, respectively, in electrical and electronic engineering from the Khulna University of Engineering & Technology, Khulna, Bangladesh, where she is currently working toward the Ph.D. degree in electrical and electronic engineering. Her research interests include smartphone-based instrumentation, and optical fiber communication.

Md Arafat Hossain received the Ph.D. degree in 2017 on smart sensing and instrumentation from The University of Sydney, Sydney, NSW, Australia, where he worked with Prof. John Canning. He is currently an Associate Professor of electrical and electronic engineering with the Khulna University of Engineering & Technology, Khulna, Bangladesh. His research interests include smart sensing, smartphone instrumentations, and 3D-printed optics. He was the recipient of the Australian Award of Endeavour Fellowship for his postdoctoral research in smart sensing.

Md Rafiqul Islam received the B.Sc. degree in electrical and electronic engineering from the Khulna University of Engineering & Technology (KUET), Khulna, Bangladesh, in 1991, the M.Sc. degree in electrical and electronic engineering from the Bangladesh University of Engineering and Technology, Dhaka, Bangladesh, in 1998, and the Doctor of Engineering degree from the Kyoto Institute of Technology, Kyoto, Japan, in 2004. Since 2007, he has been a Professor with the Department of Electrical and Electronic Engineering, KUET. His research interests include optoelectronic device modeling and simulation, optical communications, and smartphone-based instrumentation.

John Canning is currently with the University of Technology Sydney, Sydney, NSW, Australia. He has been a visiting Professor with several universities. He is a Fellow of OSA and SPIE. He was the recipient of the 2017 OSA David Richardson Medal.

Declaration of Competing Interest

The authors declare that they have no known competing financial interests or personal relationships that could have appeared to influence the work reported in this paper.

The authors declare the following financial interests/personal relationships which may be considered as potential competing interests:

Graphical abstract

